Inorganic Chemistry

pubs.acs.org/IC
Article

Coordination of XeF_2 to Fluoridometal Cations: The Adduct Cations $[PtF_3(XeF_2)_3]^+$ and $[PdF_3(XeF_2)_3]^+$

Klemen Motaln, Miha Virant, and Matic Lozinšek*

Cite This: https://doi.org/10.1021/acs.inorgchem.5c05940
Read Online

ABSTRACT: Crystals of the double salts $[Xe_2F_3][MF_3(XeF_2)_3][AsF_6]_2$ (M = Pd, Pt), prepared from anhydrous HF solutions, were characterized by low-temperature single-crystal X-ray diffraction and Raman spectroscopy. The crystal structures reveal that the compounds contain the hitherto unobserved $[MF_3(XeF_2)_3]^+$ adduct cations, which differ from all previously identified examples of XeF_2 coordination to a metal(IV) center in their mononuclear and cationic nature, as well as in the coordination of multiple XeF_2 ligands to a single metal(IV) center. Quantum-chemical calculations were performed to gain insight into the bonding and electronic structure of the $[MF_3(XeF_2)_3]^+$ adduct cations, with the optimized gas-phase geometries showing good agreement with the experimental solid-state structures. The characterized $[MF_3(XeF_2)_3]^+$ adduct cations markedly extend the chemistry of XeF_2−MF_4 systems and represent rare, crystallographically characterized examples of XeF_2 coordination to Pt^{IV} and Pd^{IV}, a feature also believed to occur in the structure of the first discovered noble-gas compound, $XePtF_6$. Moreover, the $[MF_3(XeF_2)_3]^+$ cations constitute the first examples of a new class of XeF_2 coordination compounds, which are characterized by XeF_2 ligation to a fluoridometal $[MF_x]^{n+}$ cation, thereby enabling further expansion of the coordination chemistry of noble-gas fluorides.

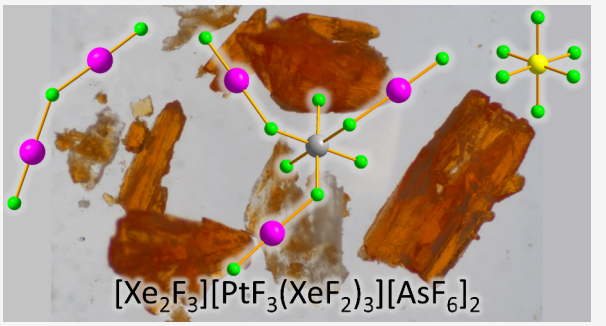

INTRODUCTION

Xenon difluoride, XeF_2, is arguably the most well-known noble-gas compound and, owing to its commercial availability, one of the most important synthetic precursors for xenon chemistry.[1] The reactivity of XeF_2 is typically governed by its pronounced Lewis basicity and fluoride-ion donor abilities.[2,3] Upon interaction with Lewis acids or fluoride-ion acceptors, XeF_2 forms a variety of complexes, adducts, and tight ion-pair salts (Figure 1),[4] exhibiting varying degrees of ionization along the following pathway: $XeF_2 \rightarrow XeF^+ + F^-$.[5] Compounds derived from metal-based Lewis acids can be qualitatively divided into three classes:

i) $[\mathbf{M^{n+}(XeF_2)_m(AF_x^-)_n}]$ **complexes**, formed by coordination of XeF_2 to a "naked" metal cation M^{n+} derived from an $M(AF_x)_n$ salt with a weakly coordinating anion, for example homoleptic $[Cu(XeF_2)_6](RuF_6)_2$, anion-bridged $[Ni(XeF_2)_2(RuF_6)_2]$,[6] and anion- and XeF_2-bridged $[Ba(XeF_2)_4(AsF_6)_2]\cdot XeF_2$ (Figure 1a).[7]

ii) $m\mathbf{XeF_2}\cdot n\mathbf{MF_x}$ **and** $m\mathbf{XeF_2}\cdot n\mathbf{MO_xF_y}$ **Lewis acid−base adducts**, formed by interaction of XeF_2 with moderately strong Lewis acids such as metal tetrafluorides and oxyfluorides, for example: $XeF_2\cdot CrF_4$,[8] $3XeF_2\cdot 2MnF_4$, $XeF_2\cdot MnF_4$,[9] $XeF_2\cdot CrOF_4$, $XeF_2\cdot 2CrOF_4$,[10] $XeF_2\cdot MoOF_4$, $XeF_2\cdot WOF_4$, $XeF_2\cdot 2WOF_4$ (Figure 1b).[11]

iii) $[\mathbf{XeF}]^+$ **tight ion-pair salts and** $[\mathbf{Xe_2F_3}]^+$ **salts**, produced in reactions with strongly Lewis acidic metal or metalloid pentafluorides, for example: $[XeF][AF_6]$ (A = As, Nb, Ru, Sb, Ta, Pt, Bi), $[XeF][A_2F_{11}]$ (A = Ru, Sb, Ta, Pt, Bi), and $[Xe_2F_3][AF_6]$ (A = As, Ru, Sb, Ta, Pt, Au, Bi) (Figure 1c).[1,4,12−15]

However, there are borderline cases that may be classified as either class (ii) or class (iii). For example, $2XeF_2\cdot 9TiF_4$ and $XeF_2\cdot 2MF_4$ (M = Mn, Pd, Pt) exhibit sufficient ionization of XeF_2 coordinated to the metal(IV) center to justify ionic formulations of $[XeF]^+_2[Ti_9F_{38}]^{2-}$ and $[XeF]^+[M_2F_9]^-$ (M = Mn, Pd, Pt), respectively (Figure 1d).[9,16,17] In contrast, crossover species between classes (i) and (ii), such as $[M^{n+}F_p(XeF_2)_m]^{(n-p)+}(AF_x^-)_{n-p}$, in which the metal center is coordinated by both XeF_2 and F^- ligands, have not been reported. Comparable linkages have been observed in the coordination chemistry of the related KrF_2, as the crystal structures of $[\mu\text{-}FHg(\mu_3\text{-}FKrF)_{1.5}(FKrF)_{0.5}AsF_6]_2$ and $[\mu_3\text{-}FHg(\mu_3\text{-}FKrF)_{0.5}(FKrF)_{1.5}AsF_6]_2$ were shown to consist of extended three-dimensional networks incorporating bridging F^- and KrF_2 units which ligate Hg^{2+} centers.[18]

Received: December 19, 2025
Revised: February 5, 2026
Accepted: February 10, 2026

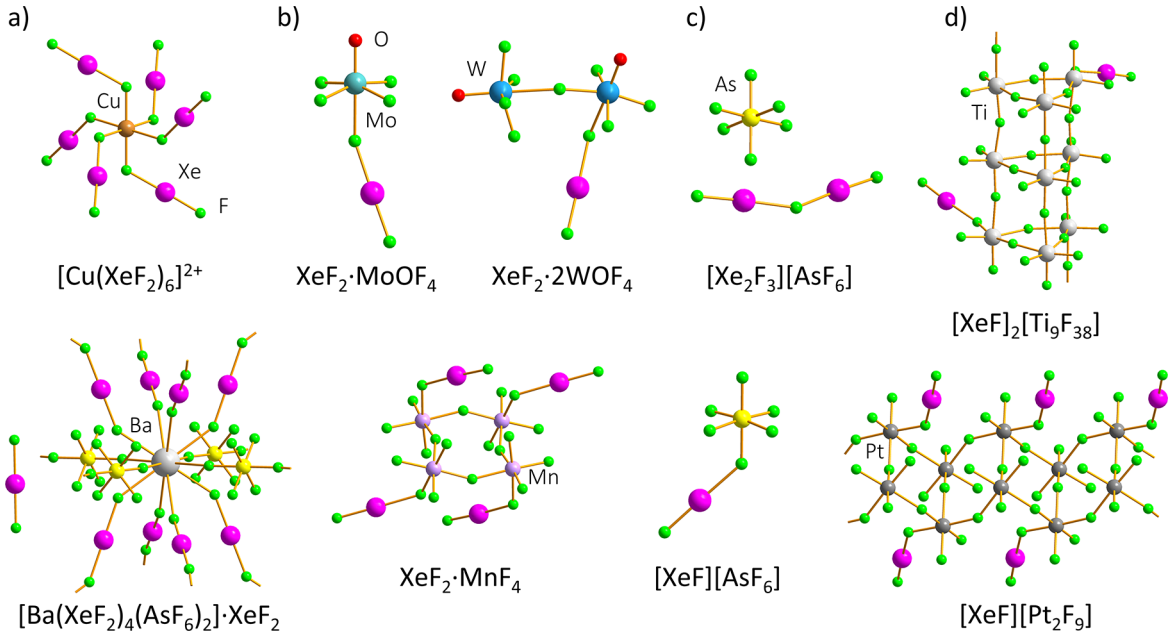

Figure 1. Structural diversity of compounds stemming from the interaction of XeF_2 with metal-based (and metalloid-based) Lewis acids.[6,7,9,11,13,15−17]

In this work, the first examples of discrete $[M^{n+}F_p(XeF_2)_m]^{(n-p)+}$ species are reported, represented by the unique $[MF_3(XeF_2)_3]^+$ (M = Pt, Pd) adduct cations, which were isolated as brightly colored crystals of the corresponding $[Xe_2F_3][MF_3(XeF_2)_3][AsF_6]_2$ double salts. Despite the fact that XeF_2 coordination to platinum constitutes a defining structural feature of the first discovered noble-gas compound, $XePtF_6$ ($XeF_2{\cdot}PtF_4$),[19,20] the structural chemistry of the XeF_2−PtF_4 system and the related[21] XeF_2−PdF_4 system remains poorly explored. The *fac*-$[M^{IV}F_3(XeF_2)_3]^+$ adduct cations described herein represent only the second instance of crystallographically characterized species featuring XeF_2 coordination to platinum and palladium, following the recently structurally characterized $XeF_2{\cdot}2PtF_4$ and $XeF_2{\cdot}2PdF_4$ adducts, whose structures were elucidated by 3D electron diffraction.[17] The newly discovered $[MF_3(XeF_2)_3]^+$ (M = Pt, Pd) adduct cations thus offer additional insights into these historically important systems.

RESULTS AND DISCUSSION

Synthesis

The title compounds were synthesized in anhydrous HF (aHF) by reactions of the appropriate binary fluorides in the molar ratios observed in the final products ($XeF_2/MF_4/AsF_5$ = 5:1:2) (eqs 1, 2).

$$5XeF_2 + PtF_4 + 2AsF_5 \xrightarrow{\text{aHF}} x[Xe_2F_3][PtF_3(XeF_2)_3][AsF_6]_2(oP256) + y[Xe_2F_3][AsF_6] \quad (1)$$

$$5XeF_2 + PdF_4 + 2AsF_5 \xrightarrow{\text{aHF}} x[Xe_2F_3][PdF_3(XeF_2)_3][AsF_6]_2 + y[Xe_2F_3][AsF_6] + z(XeF_2{\cdot}2PdF_4) \quad (2)$$

To the best of our knowledge, this approach represents a rare targeted investigation of XeF_2 reactivity in a system containing both Lewis-acidic tetra- and pentafluorides. The fluorobasic conditions established by the excess of XeF_2 ensured partial dissolution of the otherwise aHF-insoluble metal tetrafluorides, resulting in yellow-colored solutions, into which AsF_5 was subsequently dosed. Slow crystallization induced by solvent evaporation afforded amber-colored crystals (Figure S1), which were isolated and characterized by low-temperature (LT) single-crystal X-ray diffraction (SCXRD) and LT Raman spectroscopy. The formation of $[Xe_2F_3][MF_3(XeF_2)_3][AsF_6]_2$ single crystals was invariably accompanied by the formation of colorless crystals of $[Xe_2F_3][AsF_6]$, which were identified by Raman spectroscopy and SCXRD. Additional reaction pathways were explored by reacting a 2-fold molar excess of $[XeF][AsF_6]$ with K_2PtF_6, or by combining $[XeF][AsF_6]$, $XeF_2{\cdot}PdF_4$, and XeF_2 while maintaining a $XeF_2/MF_4/AsF_5$ ratio of 5:1:2 (see the Experimental Section). In both cases, the title compounds were again obtained; however, in the former reaction, a triclinic polymorph of $[Xe_2F_3][PtF_3(XeF_2)_3][AsF_6]_2$ was isolated (eq 3).

$$2[XeF][AsF_6] + K_2PtF_6 \xrightarrow{\text{aHF}} x[Xe_2F_3][PtF_3(XeF_2)_3][AsF_6]_2(aP256) + yKAsF_6 + z(nXeF_2{\cdot}PtF_4) \quad (3)$$

Crystal Structures

Structural analysis revealed that $[Xe_2F_3][PtF_3(XeF_2)_3][AsF_6]_2$, synthesized from the binary fluorides XeF_2, PtF_4, and AsF_5, crystallizes in the orthorhombic $P2_12_12_1$ space group, whereas the polymorph prepared by the reaction of $[XeF][AsF_6]$ with K_2PtF_6 crystallizes in the lower-symmetry triclinic $P\bar{1}$ space group. The two polymorphic forms are henceforth referred to by their Pearson symbols as *oP*256 and *aP*256, respectively. In contrast, crystal structure determination of $[Xe_2F_3]$-$[PdF_3(XeF_2)_3][AsF_6]_2$ revealed that it is not isotypic with

https://doi.org/10.1021/acs.inorgchem.5c05940
Inorg. Chem. XXXX, XXX, XXX−XXX

either of the $[Xe_2F_3][PtF_3(XeF_2)_3][AsF_6]_2$ polymorphs and instead crystallizes in the monoclinic $P2_1$ space group (Tables 1 and S1). Tables 1 and 2 contain the summary of crystal data and refinement results, and the selected bond lengths and angles observed in the crystal structures, respectively, whereas complete crystallographic tables are provided in the Supporting Information (Tables S1–S4).

Table 1. Summary of Crystal Data and Refinement Results for $[Xe_2F_3][PtF_3(XeF_2)_3][AsF_6]_2$(*oP*256) $[Xe_2F_3][PtF_3(XeF_2)_3][AsF_6]_2$(*aP*256), and $[Xe_2F_3][PdF_3(XeF_2)_3][AsF_6]_2$

	$[Xe_2F_3][PtF_3(XeF_2)_3][AsF_6]_2$(*oP*256)	$[Xe_2F_3][PtF_3(XeF_2)_3][AsF_6]_2$(*aP*256)	$[Xe_2F_3][PdF_3(XeF_2)_3][AsF_6]_2$
space group	$P2_12_12_1$	$P\bar{1}$	$P2_1$
a (Å)	11.86164(10)	12.92922(7)	6.53000(4)
b (Å)	16.48399(13)	13.07591(6)	11.83284(6)
c (Å)	23.8108(2)	27.91602(13)	14.93053(9)
α (°)	90	83.6237(4)	90
β (°)	90	79.6369(4)	90.0233(5)
γ (°)	90	75.7149(5)	90
V (Å^3)	4655.66(7)	4487.97(4)	1153.658(11)
Z	8	8	2
M_w (g mol^{-1})	1457.43	1457.43	1368.74
D_{calcd} (g cm^{-3})	4.159	4.314	3.940
μ (mm^{-1})	8.639	8.962	5.838
R_1	0.0389	0.0319	0.0320
wR_2	0.1001	0.0811	0.0797
$\Delta\rho_{min,\ max}$ (e Å^{-3})	−1.958, 5.733	−2.818, 4.386	−1.959, 1.990

In all structures, the asymmetric unit is comprised of isolated $[Xe_2F_3]^+$, $[MF_3(XeF_2)_3]^+$, and $[AsF_6]^-$ ions, with all atoms occupying general positions (Figures 2,3 and S2–S6). The $M^{IV}F_3^+$ fragment is coordinated by three XeF_2 ligands in a *fac* arrangement, resulting in a slightly distorted octahedral coordination environment around the M^{IV} center. These compounds, which feature three XeF_2 ligands coordinated to a single metal(IV) center, currently represent the highest number of XeF_2 ligands observed for any metal(IV) species. They also constitute a unique case in which XeF_2 coordination to a metal(IV) center results in a mononuclear complex. In contrast, the other known compounds exhibiting XeF_2 coordination to metal(IV) centers predominantly adopt polymeric structures composed of interconnected $[MF_6]$ octahedra, forming chains ($XeF_2{\cdot}CrF_4$ and $3XeF_2{\cdot}2MnF_4$),[8,9] double chains ($XeF_2{\cdot}2MnF_4$, $XeF_2{\cdot}2PdF_4$, and $XeF_2{\cdot}2PtF_4$)[9,17] (Figure 1d), columnar motifs ($[XeF]_2[Ti_9F_{38}]$)[16] (Figure 1d), or layers ($XeF_2{\cdot}2CrF_4$).[22] The sole exception within this family of compounds is $XeF_2{\cdot}MnF_4$, whose structure comprises

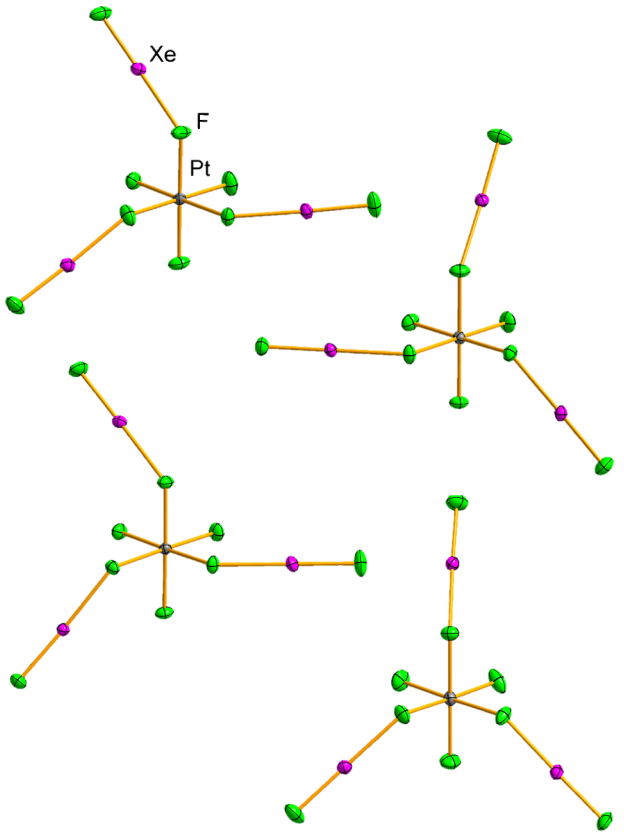

Figure 2. Four crystallographically independent $[PtF_3(XeF_2)_3]^+$ cations in the crystal structure of $[Xe_2F_3][PtF_3(XeF_2)_3][AsF_6]_2$(*aP*256). Displacement ellipsoids are drawn at the 50% probability level.

Table 2. Selected Bond Lengths (Å) and Angles (°) for the Crystal Structures of $[Xe_2F_3][PtF_3(XeF_2)_3][AsF_6]_2$ and $[Xe_2F_3][PdF_3(XeF_2)_3][AsF_6]_2$

	$[Xe_2F_3][PtF_3(XeF_2)_3][AsF_6]_2$(*oP*256)	$[Xe_2F_3][PtF_3(XeF_2)_3][AsF_6]_2$(*aP*256)	$[Xe_2F_3][PdF_3(XeF_2)_3][AsF_6]_2$
Xe−F_t	1.888(6)−1.921(6)	1.898(3)−1.918(3)	1.918(4)−1.923(4)
Xe−F_b(M)	2.182(5)−2.211(5)	2.179(3)−2.214(2)	2.143(4)−2.178(4)
Xe−F_t[a]	1.906(5)−1.929(5)	1.908(3)−1.923(3)	1.915(4), 1.916(4)
Xe−F_b(Xe)	2.125(5)−2.174(5)	2.157(3)−2.188(3)	2.142(4), 2.162(4)
M−F_t	1.881(5)−1.898(5)	1.882(3)−1.897(2)	1.842(5)−1.860(4)
M−F_b(Xe)	1.978(5)−1.996(5)	1.981(3)−2.002(2)	1.975(4)−1.990(4)
As−F	1.657(13)−1.786(13)	1.704(3)−1.737(3)	1.714(4)−1.740(4)
F−Xe−F	175.9(2)−176.8(2)	173.35(14)−179.40(12)	177.2(2)−178.2(2)
F−Xe−F[a]	177.1(3)−178.9(3)	178.11(15)−179.36(14)	178.1(2), 179.36(19)
Xe−F_b−Xe[a]	139.9(3), 140.3(3)	127.10(13)−134.65(15)	133.11(19)
cis-F−M−F	87.0(2)−93.3(2)	85.56(12)−92.53(12)	87.9(2)−92.6(3)
trans-F−M−F	178.3(2)−179.6(2)	177.12(12)−179.00(12)	178.16(19)−179.5(2)
cis-F−As−F	79.7(8)−98.3(8)	88.11(17)−91.72(15)	87.5(2)−91.2(3)
trans-F−As−F	169.0(11)−179.3(4)	177.69(17)−179.73(17)	177.4(2)−179.7(3)

[a]Pertaining to the bonds in the $[Xe_2F_3]^+$ cations.

https://doi.org/10.1021/acs.inorgchem.5c05940
Inorg. Chem. XXXX, XXX, XXX−XXX

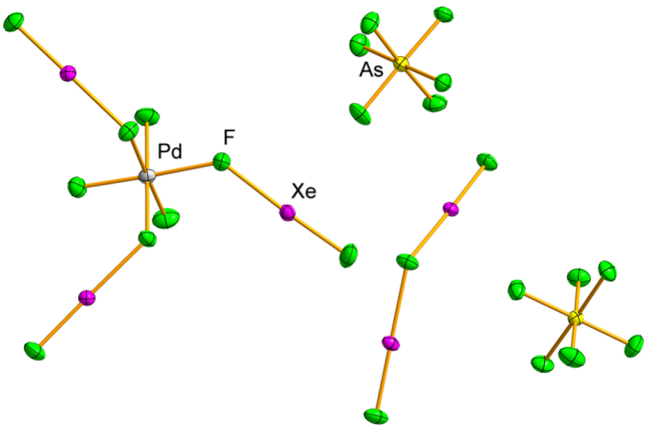

Figure 3. Asymmetric unit of the $[Xe_2F_3][PdF_3(XeF_2)_3][AsF_6]_2$ crystal structure. Displacement ellipsoids are drawn at the 50% probability level.

discrete tetrameric ring units (Figure 1b). Across all of these structures, each metal(IV) center is coordinated by no more than one XeF_2 ligand.

The geometry of the coordinated XeF_2 ligands in the $[PtF_3(XeF_2)_3]^+$ and $[PdF_3(XeF_2)_3]^+$ adduct cations is perturbed, showing slight deviations of the F−Xe−F angles from linearity [175.9(2)−176.8(2)° in *oP*256, 173.35(14)−179.35(12)° in *aP*256, and 177.2(2)−178.2(2)° in the Pd compound] and a pronounced elongation of the bridging Xe−F_b bonds, accompanied by shortening of the terminal Xe−F_t bonds. The Xe−F_t and Xe−F_b bond lengths in the $[PdF_3(XeF_2)_3]^+$ cation span the ranges of 1.918(4)−1.923(4) Å and 2.143(4)−2.178(4) Å, respectively, with average values of 1.920 and 2.159 Å. These distances indicate that the XeF_2 moiety displays an intermediate degree of ionization, comparable to that observed in some XeF_2−MF_4 adducts, namely $3XeF_2{\cdot}2MnF_4$, $XeF_2{\cdot}MnF_4$,[9] and $XeF_2{\cdot}CrF_4$.[8] For comparison, the Xe−F bond length of the centrosymmetric XeF_2 molecule ($D_{\infty h}$) in the solid state is 1.999(4) Å.[13] In the case of the $[PtF_3(XeF_2)_3]^+$ cations, a greater variability in the Xe−F bond lengths is observed. The Xe−F_t bonds measure 1.888(6)−1.921(6) Å and 1.898(3)−1.918(3) Å, whereas the Xe−F_b bonds measure 2.182(5)−2.211(5) Å and 2.179(3)−2.214(2) Å in the *oP*256 and *aP*256 polymorphs, respectively. Examination of the average values of the Xe−F_t and Xe−F_b bond lengths, which amount to 1.908 Å and 2.196 Å in the *oP*256 polymorph, and 1.908 Å and 2.200 Å in the *aP*256 polymorph, reveals a pronounced distortion of the geometry of the coordinated XeF_2 ligands. The mean values are comparable to the bond lengths observed in the [XeF][BiF_6] tight ion-pair salt [Xe−F_t: 1.913(7) Å; Xe−F_b: 2.204(7) Å],[13] providing evidence for the substantial fluoride-ion affinity of the $[PtF_3]^+$ cation. Nevertheless, the fluoride-ion affinity of these cations is

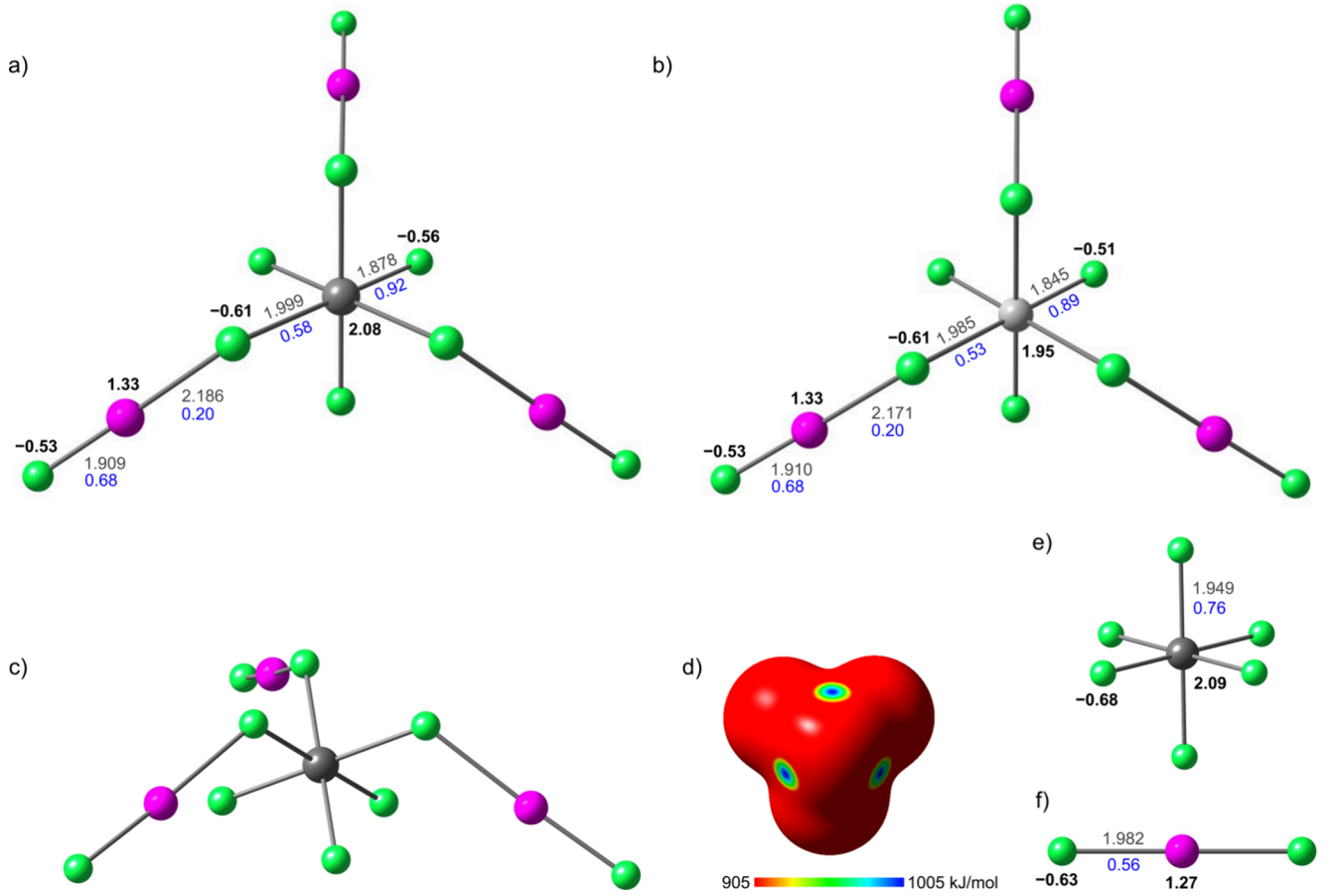

Figure 4. Calculated gas-phase geometries of (a) $[PtF_3(XeF_2)_3]^+$ and (b) $[PdF_3(XeF_2)_3]^+$ cations; (c) an alternative view of $[PtF_3(XeF_2)_3]^+$ cation; (d) molecular electrostatic potential surface (MEPS) of $[PtF_3]^+$ fragment (top 10% of the positive electrostatic potential range); and optimized gas-phase geometries of (e) $[PtF_6]^{2-}$ anion and (f) free XeF_2, included for comparison. Bond distances (Å) are indicated in gray, AIM charges are listed in black, and Mayer bond orders are given in blue.

https://doi.org/10.1021/acs.inorgchem.5c05940
Inorg. Chem. XXXX, XXX, XXX−XXX

less pronounced than that exhibited by the polymeric fluoridoplatinate(IV) and fluoridopalladate(IV) units present in the crystal structures of $XeF_2{\cdot}2MF_4$ (M = Pt, Pd), where Xe−F_b bond lengths exceeding 2.3 Å are observed.[17] The Pt−F_t [*oP*256: 1.881(5)−1.898(5) Å; *aP*256: 1.882(3)−1.897(2) Å] and Pd−F_t bond lengths [1.842(5)−1.860(5) Å] show good agreement with the values observed in the crystal structures of $XeF_2{\cdot}2PtF_4$ [1.863(7)−1.905(11) Å] and $XeF_2{\cdot}2PdF_4$ [1.844(4)−1.866(4) Å], respectively. Conversely, the bridging Pt−F_b(Xe) bond distances [*oP*256: 1.978(5)−1.996(5) Å; *aP*256: 1.981(3)−2.002(2) Å] and Pd−F_b(Xe) [1.975(4)−1.990(4) Å] are notably elongated in comparison to their counterparts observed in the crystal structures of $XeF_2{\cdot}2PtF_4$ [1.932(8) Å] and $XeF_2{\cdot}2PdF_4$ [1.894(4) Å], respectively.[17] In all three crystal structures, a number of inter- and intramolecular Xe···F contacts are formed, with distances shorter than the corresponding sum of the van der Waals radii 3.74 Å (Tables S5−S7).[23,24] These contacts contribute to stabilization of the crystal packing and influence the marked conformational differences observed among the crystallographically independent $[PtF_3(XeF_2)_3]^+$ and $[PdF_3(XeF_2)_3]^+$ adduct cations (Figure S7). In the crystal structures, the adduct cations possess C_1 point-group symmetry and are therefore chiral. As $[Xe_2F_3][PtF_3(XeF_2)_3][AsF_6]_2$(*oP*256) and $[Xe_2F_3][PdF_3(XeF_2)_3][AsF_6]_2$ crystallize in Sohncke space groups, only one enantiomeric form of each cation is present in each crystal structure. Conversely, both enantiomers of the cation are present in the centrosymmetric $P\bar{1}$ crystal structure of $[Xe_2F_3][PtF_3(XeF_2)_3][AsF_6]_2$(*aP*256).

The second cationic species present in these double salts are the planar, V-shaped $[Xe_2F_3]^+$ cations. Interestingly, the Xe−F_b−Xe angles determined in the crystal structures of $[Xe_2F_3][PtF_3(XeF_2)_3][AsF_6]_2$(*aP*256) [127.10(13)−134.65(15)°] and $[Xe_2F_3][PdF_3(XeF_2)_3][AsF_6]_2$ [133.11(19)°] (Figures S3 and 3) are the least obtuse angles observed for $[Xe_2F_3]^+$ cations to date. Previously reported fluoride-bridge angles span the range from 139.8(8)° in trigonal $[Xe_2F_3][AsF_6]$[15] to 164.3(3)° observed in the crystal structure of $[Xe_2F_3][Ti_8F_{33}]$.[16] On the other hand, the Xe−F_b−Xe angles observed in the crystal structure of $[Xe_2F_3][PtF_3(XeF_2)_3][AsF_6]_2$(*oP*256) are noticeably more open [139.9(3)° and 140.3(3)°]. As quantum-chemical calculations have previously shown that the vibrational mode corresponding to the bending deformation of the Xe−F_b−Xe angle is very low in frequency, the large variability of these angles has been ascribed to crystal-packing effects.[15]

Computational Results

To investigate the electronic structures of the isolated $[MF_3(XeF_2)_3]^+$ cations, their geometries were optimized using the DFT method PBE0-D3/aug-cc-pVQZ(-PP) as implemented in the *ORCA* software (version 6.0.0).[25] The resulting stationary points were confirmed to be true minima on the potential energy surface with no imaginary frequencies (Table S8). In the absence of additional interactions, the isolated cations examined in the computational analysis converged to a slightly distorted C_{3v} symmetry (Figure 4, Tables S9 and S10). A comparison of the experimentally determined and calculated bond lengths demonstrates good agreement, with deviations not exceeding 0.6% (Table S11 and S12). However, greater discrepancies between the experimental and calculated structures are observed in the conformation of the cations. In particular, the Xe−F_b−M angles are, on average, more acute in the calculated geometries than in the experimental structures (Tables S11 and S12). Moreover, although the Xe−F_b−M−F_t' (where F_t' denotes the terminal F atom nearest to Xe) torsion angles observed in the crystal structures span a wide range of values (Tables S2−S4), the calculated geometries converge to torsion angles that correspond to staggered conformations (Tables S11 and S12).[13]

The studied $[MF_3(XeF_2)_3]^+$ adduct cations can be described in terms of two limiting structures: one featuring neutral XeF_2 ligands coordinated to a $[MF_3]^+$ cation, and the other corresponding to complete ionization into $[XeF]^+$ cations coordinated to a $[MF_6]^{2-}$ anion.

Unbound, centrosymmetric XeF_2 is characterized by negative atoms-in-molecules (AIM) charges on the fluorine atoms (−0.63), a positive charge on the xenon atom (+1.27), and equal Mayer bond orders (0.56) for both Xe−F bonds (1.982 Å; Figure 4, Table S13). Upon coordination, XeF_2 becomes polarized, developing a net positive charge (+0.20). The terminal fluorine atom (−0.53) becomes less negative and the xenon atom (+1.33) becomes more positive, accompanied by shortening of the terminal Xe−F_t bond (1.909 Å) and an increase in the corresponding Mayer bond order (0.68). In contrast, the charge on the bridging fluorine atoms remains nearly unchanged (−0.61), while the bridging Xe−F_b bonds are significantly elongated (Pt: 2.186 Å; Pd: 2.171 Å), resulting in a decrease in the corresponding Mayer bond orders (0.20). These changes are attributed to the transfer of electron density from XeF_2 toward regions of positive electrostatic potential on the $[MF_3]^+$ fragments, which display pronounced σ-holes along the extensions of the M−F bonds (Figures 4, S8, S9 and Table S14). The coordination of XeF_2 ligands to the MF_3^+ cation can therefore be described as a regium-bonding interaction.[26]

The AIM charges of the metal centers in the adduct cations (Pt: +2.08; Pd: +1.95) are nearly identical to those calculated for the isolated $[PtF_6]^{2-}$ (+2.09) and $[PdF_6]^{2-}$ (+1.97) anions, whereas the fluorine atoms of the anions carry more negative charge (Pt: −0.68; Pd: −0.66) than either the bridging (−0.61) or terminal F atoms (Pt: −0.56; Pd: −0.51) in the adduct cations (Figure 4, Tables S15, S16). The total charge of the $[MF_6]$ fragments (−1.41) is less negative than that of the isolated $[MF_6]^{2-}$ anions (−2.00), consistent with the positive charge developed on the coordinated XeF_2 ligands (+0.59). The Mayer bond orders of the M−F_t bonds in the adduct cations (Pt: 0.92; Pd: 0.89) are significantly higher than those calculated for the M−F bonds in the $[MF_6]^{2-}$ anions (Pt: 0.76; Pd: 0.70), whereas the M−F_b bond orders in the adduct cations are smaller (Pt: 0.58; Pd: 0.53).

The topological parameters obtained from the quantum theory of atoms in molecules (QTAIM) analysis[27] (Table S17) further corroborate the polarization of XeF_2. Specifically, the Xe−F_b bond exhibits a reduced covalent character relative to uncoordinated XeF_2, as indicated by a lower electron density at the bond critical point ($\rho(r)$), a smaller Laplacian of electron density ($\nabla^2\rho(r)$), and a less negative local energy density ($H(r)$). In contrast, the Xe−F_t bond shows an enhanced covalent character, reflected in higher $\rho(r)$ values, a larger $\nabla^2\rho(r)$, and a more negative $H(r)$. The M−F_b interactions, characterized by low $\rho(r)$ values, small positive $\nabla^2\rho(r)$, and slightly negative $H(r)$ values, are consistent with predominantly electrostatic σ-hole−type interactions.[11]

https://doi.org/10.1021/acs.inorgchem.5c05940
Inorg. Chem. XXXX, XXX, XXX−XXX

Vibrational Spectroscopy

Low-temperature Raman spectra of the compounds, recorded at 100 K, exhibit the strongest bands in the Xe−F_t stretching region (580−620 cm^{-1}; Figure 5, Table S18). Given that

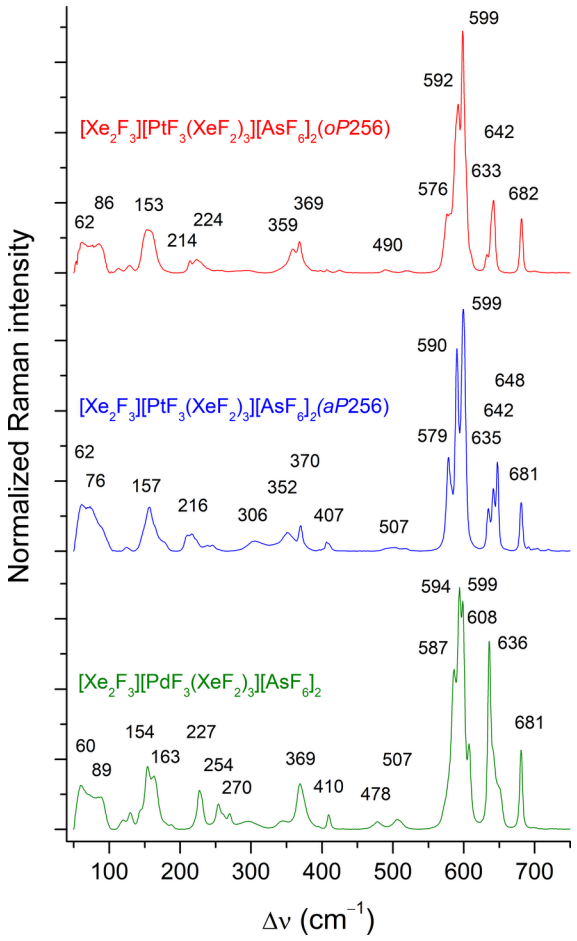

Figure 5. Raman spectra of the two polymorphs of $[Xe_2F_3][PtF_3(XeF_2)_3][AsF_6]_2$ and $[Xe_2F_3][PdF_3(XeF_2)_3][AsF_6]_2$ recorded at 100 K using 785 nm excitation.

stretching modes of both $[Xe_2F_3]^+$ and coordinated, partially ionized XeF_2 species are expected to occur in this region,[9,15,28,29] assignment of the observed bands to the respective vibrational modes is challenging. The spectra of $[Xe_2F_3][MF_3(XeF_2)_3][AsF_6]_2$ exhibit similarities to the Raman spectrum of $[Xe_2F_3][AsF_6]$, as evidenced by the nearly unchanged positions of the ν_1 (681, 682 cm^{-1}) and ν_5 bands (369, 370 cm^{-1}) of the $[AsF_6]^-$ anion in comparison to the Raman spectrum of $[Xe_2F_3][AsF_6]$, in which these bands are located at 681 and 367 cm^{-1}, respectively (Figures S10 and S11).[28] Another prominent feature of the spectra is the presence of medium-strong bands in the 630−650 cm^{-1} region. These bands correspond reasonably well to the calculated in-phase and out-of-phase M−F_t stretching modes of the $[MF_3(XeF_2)_3]^+$ cations (Table S8, Figure S10, S11). The ATR-IR spectra of samples containing $[Xe_2F_3][MF_3(XeF_2)_3][AsF_6]_2$ double salts and the spectra of pure $[Xe_2F_3][AsF_6]$ and $KAsF_6$, are provided in the Supporting Information (Figures S12 and S13).

CONCLUSIONS

In summary, two polymorphic forms of $[Xe_2F_3][PtF_3(XeF_2)_3][AsF_6]_2$, as well as $[Xe_2F_3][PdF_3(XeF_2)_3][AsF_6]_2$, were synthesized and characterized by SCXRD, vibrational spectroscopy, and quantum-chemical calculations. The novel $[MF_3(XeF_2)_3]^+$ adduct cations present in the crystal structures of these double salts provide rare, structurally characterized examples of XeF_2 coordination to platinum(IV) and palladium(IV) centers and represent the highest number of XeF_2 ligands bound to a single metal(IV) center observed to date. These findings highlight the substantial structural diversity exhibited by species in which XeF_2 ligates a tetravalent metal center.

The adduct cations identified in this study define a new class of coordination complexes in which XeF_2 serves as a ligand to a fluoridometal cation, thereby broadening the scope of XeF_2 coordination chemistry. Moreover, the results indicate that probing the reactivity of XeF_2 in systems containing multiple high-valent, Lewis-acidic fluorides can lead to the formation of novel species. This observation underscores the potential for systematic exploration across the broad landscape of mixed MF_4/AF_5−XeF_2 systems, a largely unexplored domain with a strong potential for advancing this emerging class of compounds.

EXPERIMENTAL SECTION

CAUTION: *Anhydrous HF, F_2, and AsF_5 are highly toxic volatile substances and must be handled with great care in a well-ventilated fume hood while wearing appropriate personal protective equipment at all times. XeF_2 and its derivatives are potent oxidizing fluorinating agents and release HF upon hydrolysis. Work with such chemicals should be undertaken only by properly trained experimentalists and the access to proper treatment procedures in the event of exposure must be ensured.*[30−32]

General

All experimental work on the compounds described herein was conducted under strictly anhydrous conditions. Manipulation of volatile materials was performed on a custom-built, fluorine-resistant vacuum line constructed from nickel, copper, poly(tetrafluoroethylene) (PTFE), and fluorinated ethylene propylene (FEP). Solid materials were handled in a glovebox (Vigor SG1200/750E−SG1500/750E) under an inert nitrogen atmosphere, with moisture levels maintained below 1 ppm at all times.

The syntheses of $[Xe_2F_3][MF_3(XeF_2)_3][AsF_6]_2$ compounds were carried out in h-shaped reaction vessels, constructed from two FEP tubes (6 mm i.d. × 8 mm o.d.) and equipped with either a brass-encased PTFE valve or an aluminum-encased poly(chlorotrifluoroethylene) (PCTFE) valve. The FEP tubes were heat-sealed at one end and heat-flared at the other, with one tube bent at 90° angle. The two tubes were connected to a PTFE T-section via two male-to-male PTFE connectors, with the angled side arm positioned perpendicular to the main arm. Prior to use, the reaction vessels and PTFE-coated magnetic stirring bars were passivated with 300−500 Torr of F_2 for a minimum of 8 h.

Starting Materials

Fluorine gas (Solvay Fluor, 98−99%) was used as supplied. Residual moisture was removed from commercial anhydrous HF (Linde, 99.995%) by condensing it into an FEP vessel containing K_2NiF_6 (Advance Research Chemicals, 99.9%). XeF_2 was synthesized by UV irradiation of a xenon (Messer, 99.99%) and fluorine mixture in a thoroughly dried glass bulb, employing a medium-pressure Hg lamp, as previously described.[33] AsF_5 was prepared by static fluorination of As_2O_3 in a nickel pressure vessel.[34]

Li_2PdF_6 and K_2PtF_6 were prepared by oxidation of Pd (Sigma-Aldrich, 99.9%) and Pt (Thermo Scientific, 99.98%) metals with F_2 in

https://doi.org/10.1021/acs.inorgchem.5c05940
Inorg. Chem. XXXX, XXX, XXX−XXX

aHF in the presence of LiF (Aldrich, ≥99.98%) and KF (Acros Organics, 99.99%), respectively.[35]

The synthesis of PtF_4 was conducted in accordance with the previously published procedure, commencing with the oxidation of Pt powder by XeF_2 in aHF.[36] The resulting orange-red product[17] was subsequently decomposed by heating to 430 °C in vacuo, yielding brown PtF_4, while the released XeF_2 was collected in a U-shaped FEP trap cooled with liquid nitrogen.[17]

PdF_4 was prepared by addition of AsF_5 to Li_2PdF_6 partially dissolved in aHF, following a previously reported procedure.[20,37] However, this reaction was consistently observed to yield Pd_2F_6 as a byproduct, which dominated the Raman spectrum of the isolated solid. In an attempt to synthesize high-purity PdF_4, aHF (2.0 mL) and F_2 (2.303 mmol) were condensed into a reaction vessel containing a Pd_2F_6/PdF_4 mixture (prepared from 2.293 mmol of Pd), and the vessel was placed, with agitation, under a UV light,[38] emitted from an air-cooled 1 kW Hg lamp. Following a 39-h period of UV irradiation, the product was isolated and analyzed by Raman spectroscopy. The Raman spectra revealed that the band at 566 cm^{-1}, attributable to Pd_2F_6, persisted, albeit with markedly reduced intensity. In addition, a very weak band at 1819 cm^{-1} was observed, which is likely indicative of the formation of a fluoridopalladate(IV) salt containing O_2^+ cation. A further 22-h round of UV-aided fluorination was conducted using aHF (2.0 mL) and F_2 (2.065 mmol), yet the Raman spectrum of the product remained unaltered. Nevertheless, the PXRD of the product revealed only reflections attributable to PdF_4. This material was subsequently used in the following syntheses.

$[XeF][AsF_6]$ was synthesized by condensing an equimolar amount of AsF_5 onto a frozen solution of XeF_2 in aHF.[13] The product was subsequently isolated by removal of volatiles at −45 °C using a cooled EtOH bath.

$XeF_2{\cdot}PdF_4$ was synthesized by treatment of PdF_4 with an excess of molten XeF_2, followed by removal of the excess XeF_2 under vacuum at room temperature.[17,21]

Syntheses

Synthesis of $[Xe_2F_3][PtF_3(XeF_2)_3][AsF_6]_2$(*oP*256). XeF_2 (52 mg, 0.307 mmol) and PtF_4 (14 mg, 0.052 mmol) were loaded into an h-shaped FEP vessel, and aHF (1.0 mL) was condensed onto the solids. The mixture was stirred for 20 h using a PTFE-coated magnetic stir bar, yielding a pale-yellow solution above a light-brown powder precipitate. Subsequently, AsF_5 (0.115 mmol) was condensed into the vessel, resulting in a more intense yellow coloration of the solution, while the light-brown precipitate persisted. Following an additional 2 h of stirring, the solution was decanted into the side arm, and the vessel was placed in a cooling-bath thermostat (Julabo F25-MD or Huber CC2-K6). The main arm was submerged in cooled ethanol, while the side arm containing the solution remained at room temperature. Over the subsequent 13 days, the temperature gradient between the two arms was gradually increased from 2 to 37 °C by lowering the temperature of the cooling bath, causing all aHF to evaporate from the side arm into the main arm and leaving a dark-orange solid material in the side arm. The solvent was then removed from the vessel at room temperature. Upon gentle crushing of the material isolated from the side arm, it was revealed that it consists of colorless and amber-colored crystalline chunks. SCXRD and Raman spectroscopy showed that the amber-colored and colorless crystals corresponded to $[Xe_2F_3][PtF_3(XeF_2)_3][AsF_6]_2$(*oP*256) and $[Xe_2F_3][AsF_6]$, respectively. The light-brown material remaining in the main arm exhibited PXRD pattern and Raman spectrum consistent with a mixture of PtF_4 and $[Xe_2F_3][PtF_3(XeF_2)_3][AsF_6]_2$(*oP*256).

Synthesis of $[Xe_2F_3][PtF_3(XeF_2)_3][AsF_6]_2$(*aP*256). In a typical experiment, $[XeF][AsF_6]$ (49 mg, 0.144 mmol) and K_2PtF_6 (21 mg, 0.054 mmol) were loaded into an h-shaped FEP vessel, and aHF (0.8 mL) was dispensed onto the reactants under static vacuum. Initially, a pale-orange solution formed above an orange−red solid. Upon overnight stirring, the orange-red solid converted into a tan-colored, powdered precipitate. The solution was then decanted into the side arm, and the main arm was placed in a cooling bath thermostat. The temperature gradient between the two arms was gradually increased from 4 to 46 °C over a period of 12 days, resulting in the growth of a large colorless crystal of $KAsF_6$ surrounded by orange crystalline material of $[Xe_2F_3][PtF_3(XeF_2)_3][AsF_6]_2$(*aP*256), which were analyzed by SCXRD and Raman spectroscopy. The residual tan-colored material in the main arm exhibited no powder diffraction lines and displayed a Raman spectrum matching that reported for $nXeF_2{\cdot}PtF_4$ ($1 < n < 1.6$).[17]

Synthesis of $[Xe_2F_3][PdF_3(XeF_2)_3][AsF_6]_2$ from XeF_2, PdF_4, and AsF_5 in aHF. XeF_2 (73 mg, 0.431 mmol) and PdF_4 (14 mg, 0.077 mmol) were loaded into an FEP reaction vessel, followed by the addition of aHF (1.0 mL). After stirring for 24 h, most of the brick-red PdF_4 had dissolved, affording a pale-yellow solution above a small amount of insoluble brown material. Subsequent addition of AsF_5 (0.189 mmol) produced a solution with a more intense yellow coloration, although some insoluble residue remained at the bottom of the vessel. The clear yellow supernatant was transferred to the side arm, and the main arm of the h-shaped vessel was immersed in a cooling-bath thermostat. The temperature difference between the two arms was increased from 6 to 39 °C over a period of 8 days. The resulting solid orange material in the side arm consisted of colorless crystals of $[Xe_2F_3][AsF_6]$ and amber-colored crystals of $[Xe_2F_3][PdF_3(XeF_2)_3][AsF_6]_2$, whereas Raman spectra of the brown solid remaining in the main arm indicated a mixture of $XeF_2{\cdot}2PdF_4$, $[Xe_2F_3][AsF_6]$, PdF_4, and Pd_2F_6.

Synthesis of $[Xe_2F_3][PdF_3(XeF_2)_3][AsF_6]_2$ from $[XeF][AsF_6]$, $XeF_2{\cdot}PdF_4$, and XeF_2 in aHF. The main arm of an h-shaped FEP vessel was loaded with $[XeF][AsF_6]$ (35 mg, 0.103 mmol), $XeF_2{\cdot}PdF_4$ (18 mg, 0.051 mmol), XeF_2 (19 mg, 0.112 mmol), and aHF (1 mL). The mixture was stirred for 90 min, producing a yellow solution and a dark-brown solid precipitate that adhered to the magnetic stirring bar. The solution was decanted into the side arm of the FEP vessel, and the main arm was placed in a cooling-bath thermostat. As the temperature gradient between the arms increased from 5 to 34 °C over the course of 8 days, the solvent gradually evaporated back into the main arm, leaving a solid amber-colored material in the side arm. SCXRD and Raman spectroscopy demonstrated that the amber-colored solid was composed of $[Xe_2F_3][PdF_3(XeF_2)_3][AsF_6]_2$ and $[Xe_2F_3][AsF_6]$, whereas Raman spectra of the aHF-insoluble brown material remaining in the main arm indicated that it consisted of $XeF_2{\cdot}2PdF_4$ and Pd_2F_6. The crystal of $[Xe_2F_3][PdF_3(XeF_2)_3][AsF_6]_2$ used for structural characterization by SCXRD was obtained from this preparation.

Single-Crystal X-Ray Diffraction

Crystal Mounting. Crystalline samples were placed on a watch glass and submerged in inert perfluorodecalin oil (ABCR, AB102850, 98%, *cis* and *trans*) inside an inert-atmosphere glovebox. Suitable crystals were selected under polarized light using a stereomicroscope outside the glovebox and attached to a MiTeGen dual-thickness polymer loop. Immediately after the pin was lifted above the surface of the perfluorodecalin, it was grasped with cryo-pin tongs cooled to −196 °C and rapidly transferred to the goniometer head of the diffractometer, where the crystal was protected by a stream of cold nitrogen gas (Oxford Cryosystems 800 Series Cryostream).

X-Ray Data Collection, Data Reduction, and Structure Solution. Single-crystal X-ray diffraction data was collected at low temperature (100 K) on a Rigaku OD XtaLAB Synergy-S diffractometer equipped with a Dectris EIGER2 R CdTe 1M hybrid pixel array detector using microfocused Ag *Kα* radiation (λ = 0.56087 Å). *CrysAlisPro* software was employed for data processing, utilizing empirical and numerical absorption correction.[39] The crystal structure of $[Xe_2F_3][PtF_3(XeF_2)_3][AsF_6]_2$(*oP*256) was solved using *SUPERFLIP*,[40] whereas the crystal structures of $[Xe_2F_3][PtF_3(XeF_2)_3][AsF_6]_2$(*aP*256) and $[Xe_2F_3][PdF_3(XeF_2)_3][AsF_6]_2$ were solved using *SHELXT*.[41] All three structures were refined with *SHELXL*[42] within the *Olex2* software.[43] Tabulated distances of the nonbonded Xe···F contacts were calculated using the *PLATON* program.[44] Figures were generated using the *DIAMOND* software.[45]

Because the $[Xe_2F_3][PtF_3(XeF_2)_3][AsF_6]_2$(*oP*256) crystals were always found attached to the colorless byproduct $[Xe_2F_3][AsF_6]$,

https://doi.org/10.1021/acs.inorgchem.5c05940
Inorg. Chem. XXXX, XXX, XXX−XXX

some reflections attributable to the unit cell of the latter were observed after data collection. However, application of a multicrystal data treatment resulted in a structure with inferior agreement parameters. Crystals of $[Xe_2F_3][PtF_3(XeF_2)_3][AsF_6]_2$(*oP*256) and $[Xe_2F_3][PdF_3(XeF_2)_3][AsF_6]_2$ were also found to be twinned. Furthermore, crystals of the *oP*256 and *aP*256 polymorphs of $[Xe_2F_3][PtF_3(XeF_2)_3][AsF_6]_2$ diffracted weakly at high theta angles. Accordingly, the data sets were truncated at resolutions of 0.55 Å and 0.60 Å, respectively.

One symmetry-inequivalent $[AsF_6]^-$ anion in the crystal structure of $[Xe_2F_3][PtF_3(XeF_2)_3][AsF_6]_2$(*oP*256) exhibited disorder, which was treated by splitting four axial atoms and applying SADI and RIGU restraints during refinement.

Vibrational Spectroscopy

Raman Spectroscopy. Raman spectra were measured at 100 K using a Bruker Senterra II confocal Raman microscope equipped with a Linkam LTS420 low-temperature stage. The samples were excited using a 785 nm laser at either 25 mW in the case of $[Xe_2F_3][PtF_3(XeF_2)_3][AsF_6]_2$(*oP*256) or 50 mW in the case of $[Xe_2F_3][PtF_3(XeF_2)_3][AsF_6]_2$(*aP*256) and $[Xe_2F_3][PdF_3(XeF_2)_3][AsF_6]_2$. Spectra were measured over the 50−1410 cm^{-1} range with a spectral resolution of 1.5 cm^{-1} using a 50 μm aperture. Samples were prepared by coarsely homogenizing the reaction products in an agate mortar inside a glovebox and loading the material into quartz capillaries, which had been thoroughly dried and passivated with elemental F_2 beforehand. Crystals of the $[MF_3(XeF_2)_3]^+$ salts invariably formed in the presence of $[Xe_2F_3][AsF_6]$ and $KAsF_6$ byproducts and could not be readily separated. Consequently, Raman spectra of the target compounds were obtained from isolated, brightly colored crystalline particulates that could be visually distinguished from the colorless $[Xe_2F_3][AsF_6]$ or $KAsF_6$ crystals. The plotted spectra (Figure 5) were obtained by averaging spectra from multiple, distinct, randomly oriented crystallites. The number of averaged spectra was 7 for both the *oP*256 and *aP*256 polymorphs of $[Xe_2F_3][PtF_3(XeF_2)_3][AsF_6]_2$ and 13 for $[Xe_2F_3][PdF_3(XeF_2)_3][AsF_6]_2$.

Infrared Spectroscopy. ATR-IR spectra were measured on a Bruker Alpha II FT-IR spectrometer equipped with a Platinum Diamond-ATR sampling module, operated inside an N_2-atmosphere glovebox. Spectra were measured by accumulation of 24 scans over the 400−4000 cm^{-1} range at a resolution of 4 cm^{-1}. The spectra were obtained from finely pulverized materials, which consisted of mixtures of the $[MF_3(XeF_2)_3]^+$ salts and $[Xe_2F_3][AsF_6]$ or $KAsF_6$ byproducts (Figure S12). For comparison, ATR-IR spectra of pure $[Xe_2F_3][AsF_6]$ and $KAsF_6$ were also recorded under identical conditions (Figure S13).

Computational Details

Quantum-chemical calculations were carried out using density functional theory (DFT) as implemented in the *ORCA* software package (version 6.0.0).[25,46,47] The electronic structures of the $[MF_3(XeF_2)_3]^+$ cations were calculated starting from the crystallographic coordinates and converged to stationary points with all vibrational frequencies real. The calculations were performed using the PBE0-D3 functional,[48−51] aug-cc-pVQZ for F, and aug-cc-pVQZ-PP basis sets with SK-MCDHF-RSC effective core potentials for the heavy atoms Pd,[52] Pt,[53] and Xe.[54]

Raman spectra were calculated using numerical frequency calculations (!NumFreq) together with polarizability calculations (% elprop Polar 1 end).[55] Raman intensities were calculated using the *ChemCraft*[56] Raman spectra utility with a temperature of 298.15 K and incident laser frequency of 10,000 cm^{-1}. Gaussian broadening with a full width at half-maximum of 2 cm^{-1} was applied.

Computational results were processed using the *Multiwfn* software[57,58] (version 3.8(dev)) to perform Mayer bond order analysis,[59,60] and quantitative molecular surface analyses.[27,61,62] *GaussView*[63] was used to visualize the MEPS.

■ ASSOCIATED CONTENT

Data Availability Statement

The data supporting the findings of this study are available in the Zenodo open repository (https://zenodo.org/) under the DOI number: 10.5281/zenodo.17787891.

Supporting Information

The Supporting Information is available free of charge at https://pubs.acs.org/doi/10.1021/acs.inorgchem.5c05940.

Additional crystallographic data and figures, DFT-calculated vibrational frequencies and structural parameters of the $[MF_3(XeF_2)_3]^+$ cations and their comparison with experimental values, a table of observed Raman band positions and their relative intensities, and ATR-IR spectra (PDF)

Accession Codes

Deposition Numbers 2517118−2517120 contain the supplementary crystallographic data for this paper. These data can be obtained free of charge via the joint Cambridge Crystallographic Data Centre (CCDC) and Fachinformationszentrum Karlsruhe Access Structures service.

■ AUTHOR INFORMATION

Corresponding Author

Matic Lozinšek − *Extreme Conditions Chemistry Laboratory (ECCL K2), Jožef Stefan Institute, 1000 Ljubljana, Slovenia; Jožef Stefan International Postgraduate School, 1000 Ljubljana, Slovenia;* orcid.org/0000-0002-1864-4248; Email: matic.lozinsek@ijs.si

Authors

Klemen Motaln − *Extreme Conditions Chemistry Laboratory (ECCL K2), Jožef Stefan Institute, 1000 Ljubljana, Slovenia; Jožef Stefan International Postgraduate School, 1000 Ljubljana, Slovenia;* orcid.org/0000-0003-0051-8611

Miha Virant − *Extreme Conditions Chemistry Laboratory (ECCL K2), Jožef Stefan Institute, 1000 Ljubljana, Slovenia;* orcid.org/0000-0002-5919-3631

Complete contact information is available at: https://pubs.acs.org/10.1021/acs.inorgchem.5c05940

Notes

The authors declare no competing financial interest.

■ ACKNOWLEDGMENTS

The authors gratefully acknowledge financial support from the European Research Council (ERC) under the European Union's Horizon 2020 Research and Innovation Programme (Starting Grant 950625), the Slovenian Research and Innovation Agency (ARIS) (Grant N1-0189), and the Jožef Stefan Institute Director's Fund.

■ DEDICATION

In memory of Professor Dr. Boris Frlec (1936−2026).

■ REFERENCES

(1) Tramšek, M.; Žemva, B. Synthesis, Properties and Chemistry of Xenon(II) Fluoride. *Acta Chim. Slov.* **2006**, *53*, 105−116.

(2) Bartlett, N.; Sladky, F. O. The Relative Fluoride Ion Donor Abilities of XeF_2, XeF_4, and XeF_6 and a Chemical Purification of XeF_4. *J. Am. Chem. Soc.* **1968**, *90* (19), 5316−5317.

(3) Uran, E.; Lozinšek, M. Hydrogen-Bonded Salt Cocrystals of Xenon Difluoride and Protonated Perfluoroamides. *CrystEngComm* **2025**, *27* (48), 7776−7784.
(4) Žemva, B. Binary Fluorides of Noble-Gases and Their Compounds. *Croat. Chem. Acta* **1988**, *61* (1), 163−187.
(5) Žemva, B.; Jesih, A.; Templeton, D. H.; Zalkin, A.; Cheetham, A. K.; Bartlett, N. Phases in the System XeF_2/XeF_5AsF_6 and Structural and Vibrational Evidence for the Following Ionization Pathway: $XeF_2 \rightarrow XeF^+ + F^-$. *J. Am. Chem. Soc.* **1987**, *109* (24), 7420−7427.
(6) Mrzljak, T.; Goreshnik, E.; Tavčar, G.; Tramšek, M. Coordination Chemistry of Copper and Nickel with Xenon Difluoride and the Hexafluororuthenate(V) Anion: Synthesis and Structural Studies. *Eur. J. Inorg. Chem.* **2025**, *28* (24), No. e202500275.
(7) Gerken, M.; Hazendonk, P.; Iuga, A.; Nieboer, J.; Tramšek, M.; Goreshnik, E.; Žemva, B.; Zheng, S.; Autschbach, J. Solid-State NMR Spectroscopic Study of Coordination Compounds of XeF_2 with Metal Cations and the Crystal Structure of $[Ba(XeF_2)_5][AsF_6]_2$. *Inorg. Chem.* **2007**, *46* (15), 6069−6077.
(8) Lutar, K.; Leban, I.; Ogrin, T.; Žemva, B. $XeF_2{\cdot}CrF_4$ and $(XeF_5^+CrF_5^-)_4{\cdot}XeF_4$: Syntheses, Crystal Structures and Some Properties. *Eur. J. Solid State Inorg. Chem.* **1992**, *29*, 713−727.
(9) Motaln, K.; Gurung, K.; Brázda, P.; Kokalj, A.; Radan, K.; Dragomir, M.; Žemva, B.; Palatinus, L.; Lozinšek, M. Reactive Noble-Gas Compounds Explored by 3D Electron Diffraction: XeF_2-MnF_4 Adducts and a Facile Sample Handling Procedure. *ACS Cent. Sci.* **2024**, *10* (9), 1733−1741.
(10) Mercier, H. P. A.; Breddemann, U.; Brock, D. S.; Bortolus, M. R.; Schrobilgen, G. J. Syntheses, Structures, and Bonding of $NgF_2{\cdot}CrOF_4$, $NgF_2{\cdot}2CrOF_4$ (Ng = Kr, Xe), and $(CrOF_4)_\infty$. *Chem.−Eur. J.* **2019**, *25* (52), 12105−12119.
(11) Bortolus, M. R.; Mercier, H. P. A.; Brock, D. S.; Schrobilgen, G. J. Noble-Gas Difluoride Complexes of MOF_4 (M = Mo, W); Syntheses, Structures and Bonding of $NgF_2{\cdot}MOF_4$ and $XeF_2{\cdot}2MOF_4$ (Ng = Kr, Xe). *Chem.−Eur. J.* **2022**, *28* (15), No. e202103729.
(12) Frlec, B.; Holloway, J. H. The XeF_2-MF_5 (M = Sb, Ta, or Nb) Systems: Vibrational Spectra of Solid Xenon Difluoride Adducts. *J. Chem. Soc., Dalton Trans.* **1975**, No. 6, 535−540.
(13) Elliott, H. St. A.; Lehmann, J. F.; Mercier, H. P. A.; Jenkins, H. D. B.; Schrobilgen, G. J. X-Ray Crystal Structures of $[XeF][MF_6]$ (M = As, Sb, Bi), $[XeF][M_2F_{11}]$ (M = Sb, Bi) and Estimated Thermochemical Data and Predicted Stabilities for Noble-Gas Fluorocation Salts Using Volume-Based Thermodynamics. *Inorg. Chem.* **2010**, *49* (18), 8504−8523.
(14) Gillespie, R. J.; Martin, D.; Schrobilgen, G. J. A Raman Spectroscopic Study of Noble-Gas Fluoride Adduct Formation with Bismuth Pentafluoride. *J. Chem. Soc., Dalton Trans.* **1980**, No. 10, 1898−1903.
(15) Fir, B. A.; Gerken, M.; Pointner, B. E.; Mercier, H. P. A.; Dixon, D. A.; Schrobilgen, G. J. An X-Ray Crystallographic Study of $[Xe_2F_3][SbF_6]$ and Dimorphism in $[Xe_2F_3][AsF_6]$; and a Density Functional Theory Study of the $Xe_2F_3^+$ Cation. *J. Fluorine Chem.* **2000**, *105* (1), 159−167.
(16) Radan, K.; Goreshnik, E.; Žemva, B. Xenon(II) Polyfluoridotitanates(IV): Synthesis and Structural Characterization of $[Xe_2F_3]^+$ and $[XeF]^+$ Salts. *Angew. Chem. Int. Ed.* **2014**, *53* (50), 13715−13719.
(17) Motaln, K.; Gurung, K.; Dragomir, M.; Kurzydłowski, D.; Palatinus, L.; Lozinšek, M. Crystal Structures of $XeF_2{\cdot}2PtF_4$ and $XeF_2{\cdot}2PdF_4$ Determined by 3D Electron Diffraction and Structural Models of $XePtF_6$. *Inorg. Chem.* **2025**, *64* (29), 14968−14976.
(18) De Backere, J. R.; Mercier, H. P. A.; Schrobilgen, G. J. A Structurally Diverse Series of Eight-Coordinate Hg^{2+} Complexes of KrF_2 Derived from $Hg(PnF_6)_2$ (Pn = As, Sb) and $FHg(AsF_6)$. *Inorg. Chem.* **2025**, *64* (29), 15234−15247.
(19) Bartlett, N. Xenon Hexafluoroplatinate(V) $Xe^+[PtF_6]^-$. *Proc. Chem. Soc.* **1962**, 218.
(20) Graham, L.; Graudejus, O.; Jha, N. K.; Bartlett, N. Concerning the Nature of $XePtF_6$. *Coord. Chem. Rev.* **2000**, *197* (1), 321−334.
(21) Bartlett, N.; Žemva, B.; Graham, L. Redox Reactions in the XeF_2/Platinum Fluoride and XeF_2/Palladium Fluoride Systems and the Conversion of XeF_2 to XeF_4 and Xe. *J. Fluorine Chem.* **1976**, *7* (1), 301−320.
(22) Lutar, K.; Borrmann, H.; Žemva, B. $XeF_2{\cdot}2CrF_4$ and $XeF_5^+CrF_5^-$: Syntheses, Crystal Structures, and Some Properties. *Inorg. Chem.* **1998**, *37* (12), 3002−3006.
(23) Alvarez, S. A Cartography of the van Der Waals Territories. *Dalton Trans.* **2013**, *42* (24), 8617−8636.
(24) Vogt, J.; Alvarez, S. Van Der Waals Radii of Noble Gases. *Inorg. Chem.* **2014**, *53* (17), 9260−9266.
(25) Neese, F. The ORCA Program System. *Wiley Interdiscip. Rev.: Comput. Mol. Sci.* **2012**, *2* (1), 73−78.
(26) Arunan, E.; Metrangolo, P.; Resnati, G.; Scheiner, S. IUPAC Recommendations: (Un)Equivocal Understanding of Hydrogen and Halogen Bonds and Their (Un)Equivocal Naming! *Cryst. Growth Des.* **2024**, *24* (20), 8153−8158.
(27) Bader, R. F. W. *Atoms in Molecules: A Quantum Theory*; Oxford University Press: Oxford, 1990.
(28) Gillespie, R. J.; Landa, B. Raman Spectra of Some Xenon(II) Compounds. *Inorg. Chem.* **1973**, *12* (6), 1383−1389.
(29) Milićev, S.; Lutar, K.; Žemva, B.; Ogrin, T. Vibrational Spectra of Solid CrF_4 and of Three New Fluorochromate(IV) Complexes with Xe Fluorides, $XeF_2{\cdot}CrF_4$, $(XeF_5^+CrF_5^-)_4{\cdot}XeF_4$ and $XeF_5^+CrF_5^-$. *J. Mol. Struct.* **1994**, *323*, 1−6.
(30) Peters, D.; Miethchen, R. Symptoms and Treatment of Hydrogen Fluoride Injuries. *J. Fluorine Chem.* **1996**, *79* (2), 161−165.
(31) Segal, E. B. First Aid for a Unique Acid, HF: A Sequel. *Chem. Health Saf.* **2000**, *7* (1), 18−23.
(32) Möbs, M.; Kraus, F. Tips and Procedures for Safe Handling of Anhydrous Hydrogen Fluoride and Pure Elemental Fluorine in Chemical University Laboratories. *ACS Chem. Health Saf.* **2025**, *32* (55), 662−672.
(33) Šmalc, A.; Lutar, K. Xenon Difluoride (Modification). In *Inorganic Syntheses*; Grimes, R. N., Ed.; John Wiley & Sons, 1992; Vol. *29*, pp 1−4.
(34) Mazej, Z.; Žemva, B. Synthesis of Arsenic Pentafluoride by Static Fluorination of As_2O_3 in a Closed System. *J. Fluorine Chem.* **2005**, *126* (9), 1432−1434.
(35) Lucier, G. M.; Elder, S. H.; Chacon, L.; Bartlett, N. The Room Temperature Oxidation of Gold, Ruthenium, Osmium, Iridium, Platinum, or Palladium with Fluorine in Anhydrous Hydrogen Fluoride. *Eur. J. Solid State Inorg. Chem.* **1996**, *33*, 809−820.
(36) Drews, T.; Rusch, D.; Seidel, S.; Willemsen, S.; Seppelt, K. Systematic Reactions of $[Pt(PF_3)_4]$. *Chem.−Eur. J.* **2008**, *14* (14), 4280−4286.
(37) Casteel, W. J.; Lohmann, D. H.; Bartlett, N. Room Temperature Preparations of Second and Third Transition Series Tetrafluorides and a Possible Novel Structure Type for OsF_4 and RhF_4. *J. Fluorine Chem.* **2001**, *112* (2), 165−171.
(38) Mazej, Z. Photochemical Syntheses of Fluorides in Liquid Anhydrous Hydrogen Fluoride. In *Modern Synthesis Processes and Reactivity of Fluorinated Compounds*; Groult, H.; Leroux, F. R.; Tressaud, A., Eds.; Elsevier, 2017; pp 587−607.
(39) Rigaku, OD *CrysAlisPro*; Rigaku Corporation: Wrocław, Poland, 2025.
(40) Palatinus, L.; Chapuis, G. *SUPERFLIP* − a Computer Program for the Solution of Crystal Structures by Charge Flipping in Arbitrary Dimensions. *J. Appl. Crystallogr.* **2007**, *40* (4), 786−790.
(41) Sheldrick, G. M. *SHELXT* − Integrated Space-Group and Crystal-Structure Determination. *Acta Crystallogr. A* **2015**, *71* (1), 3−8.
(42) Sheldrick, G. M. Crystal Structure Refinement with *SHELXL*. *Acta Crystallogr. C* **2015**, *71* (1), 3−8.
(43) Dolomanov, O. V.; Bourhis, L. J.; Gildea, R. J.; Howard, J. a. K.; Puschmann, H. *OLEX2*: A Complete Structure Solution, Refinement and Analysis Program. *J. Appl. Crystallogr.* **2009**, *42* (2), 339−341.
(44) Spek, A. L. Single-Crystal Structure Validation with the Program *PLATON*. *J. Appl. Crystallogr.* **2003**, *36* (1), 7−13.

https://doi.org/10.1021/acs.inorgchem.5c05940
Inorg. Chem. XXXX, XXX, XXX−XXX

(45) Putz, H.; Brandenburg, K. *Diamond – Crystal and Molecular Structure Visualization*, 2025.
(46) Neese, F. Software Update: The ORCA Program System—Version 5.0. *Wiley Interdiscip. Rev.: Comput. Mol. Sci.* **2022**, *12* (5), No. e1606.
(47) Neese, F. Software Update: The ORCA Program System—Version 6.0. *Wiley Interdiscip. Rev.: Comput. Mol. Sci.* **2025**, *15* (2), No. e70019.
(48) Adamo, C.; Barone, V. Toward Reliable Density Functional Methods without Adjustable Parameters: The PBE0 Model. *J. Chem. Phys.* **1999**, *110* (13), 6158–6170.
(49) Grimme, S.; Antony, J.; Ehrlich, S.; Krieg, H. A Consistent and Accurate Ab Initio Parametrization of Density Functional Dispersion Correction (DFT-D) for the 94 Elements H-Pu. *J. Chem. Phys.* **2010**, *132* (15), 154104.
(50) Grimme, S.; Ehrlich, S.; Goerigk, L. Effect of the Damping Function in Dispersion Corrected Density Functional Theory. *J. Comput. Chem.* **2011**, *32* (7), 1456–1465.
(51) Kendall, R. A.; Dunning, T. H., Jr.; Harrison, R. J. Electron Affinities of the First-row Atoms Revisited. Systematic Basis Sets and Wave Functions. *J. Chem. Phys.* **1992**, *96* (9), 6796–6806.
(52) Peterson, K. A.; Figgen, D.; Dolg, M.; Stoll, H. Energy-Consistent Relativistic Pseudopotentials and Correlation Consistent Basis Sets for the 4*d* Elements Y–Pd. *J. Chem. Phys.* **2007**, *126* (12), 124101.
(53) Figgen, D.; Peterson, K. A.; Dolg, M.; Stoll, H. Energy-Consistent Pseudopotentials and Correlation Consistent Basis Sets for the 5*d* Elements Hf–Pt. *J. Chem. Phys.* **2009**, *130* (16), 164108.
(54) Peterson, K. A.; Figgen, D.; Goll, E.; Stoll, H.; Dolg, M. Systematically Convergent Basis Sets with Relativistic Pseudopotentials. II. Small-Core Pseudopotentials and Correlation Consistent Basis Sets for the Post-*d* Group 16–18 Elements. *J. Chem. Phys.* **2003**, *119* (21), 11113–11123.
(55) Bykov, D.; Petrenko, T.; Izsák, R.; Kossmann, S.; Becker, U.; Valeev, E.; Neese, F. Efficient Implementation of the Analytic Second Derivatives of Hartree–Fock and Hybrid DFT Energies: A Detailed Analysis of Different Approximations. *Mol. Phys.* **2015**, *113* (13–14), 1961–1977.
(56) Zhurko, G. A. *Chemcraft - Graphical Program for Visualization of Quantum Chemistry Computations*, 2005. https://chemcraftprog.com/.
(57) Lu, T.; Chen, F. Multiwfn: A Multifunctional Wavefunction Analyzer. *J. Comput. Chem.* **2012**, *33* (5), 580–592.
(58) Lu, T. A Comprehensive Electron Wavefunction Analysis Toolbox for Chemists, Multiwfn. *J. Chem. Phys.* **2024**, *161* (8), No. 082503.
(59) Mayer, I. Charge, Bond Order and Valence in the AB Initio SCF Theory. *Chem. Phys. Lett.* **1983**, *97* (3), 270–274.
(60) Mayer, I. Improved Definition of Bond Orders for Correlated Wave Functions. *Chem. Phys. Lett.* **2012**, *544*, 83–86.
(61) Lu, T.; Chen, F. Quantitative Analysis of Molecular Surface Based on Improved Marching Tetrahedra Algorithm. *J. Mol. Graphics Modell.* **2012**, *38*, 314–323.
(62) Zhang, J.; Lu, T. Efficient Evaluation of Electrostatic Potential with Computerized Optimized Code. *Phys. Chem. Chem. Phys.* **2021**, *23* (36), 20323–20328.
(63) Dennington, R.; Keith, T. A.; Millam, J. M. *GaussView, Version 6.1.1*, 2016.

https://doi.org/10.1021/acs.inorgchem.5c05940
Inorg. Chem. XXXX, XXX, XXX–XXX